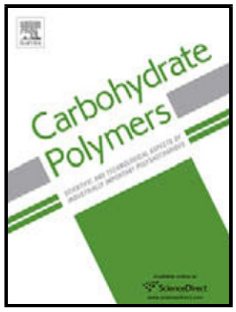

Title: Strong and electrically conductive nanopaper from cellulose nanofibers and polypyrrole

Author: Makara Lay J. Alberto Méndez Marc Delgado-Aguilar Kim Ngun Bun Fabiola Vilaseca

PII: S0144-8617(16)30777-9
DOI: http://dx.doi.org/doi:10.1016/j.carbpol.2016.06.102
Reference: CARP 11287

To appear in:

Received date: 17-5-2016
Accepted date: 27-6-2016

Please cite this article as: Lay, Makara., Méndez, J Alberto., Delgado-Aguilar, Marc., Bun, Kim Ngun., & Vilaseca, Fabiola., Strong and electrically conductive nanopaper from cellulose nanofibers and polypyrrole.*Carbohydrate Polymers* http://dx.doi.org/10.1016/j.carbpol.2016.06.102

Research highlights

Homogeneous coating of polypyrrole on cellulose nanostructure
Flexible and strong cellulose nanopaper with electrical activity
Nanopaper with 5.2 10^{-2} S cm^{-1} conductivity and 7.4 F g^{-1} specific capacitance

Strong and electrically conductive nanopaper from cellulose nanofibers and polypyrrole

Makara Lay,[a,b] J. Alberto Méndez,[a] Marc Delgado-Aguilar,[a] Kim Ngun Bun[b], Fabiola Vilaseca [a*]

a. LEPAMAP GROUP, Dept. of Chemical Engineering, Agricultural and Food Technology, Universitat de Girona, 17071 Girona, Spain.

b. Dept. of Geo-resources and Geotechnical Engineering, Institute of Technology of Cambodia, PP Box 86, Russian conf. Blvd. Phnom Penh, Cambodia.

*fabiola.vilaseca@udg.edu

Abstract

In this work, we prepare cellulose nanopapers of high mechanical performance and with the electrical conductivity of a semiconductor. Cellulose nanofibers (CNF) from bleached softwood pulp were coated with polypyrrole (PPy) via in situ chemical polymerization, in presence of iron chloride (III) as oxidant agent. The structure and morphology of nanopapers were studied, as well as their thermal, mechanical and conductive properties. Nanopaper from pure CNF exhibited a very high tensile response (224 MPa tensile strength and 14.5 GPa elastic modulus). The addition of up to maximum 20% of polypyrrole gave CNF/PPy nanopapers of high flexibility and still good mechanical properties (94 MPa strength and 8.8 GPa modulus). The electrical conductivity of the resulting CNF/PPy nanopaper was of 5.2 10^{-2} S cm^{-1}, with a specific capacitance of 7.4 F g^{-1}. The final materials are strong and conductive nanopapers that can find application as biodegradable flexible thin-film transistor (TFT) or as flexible biosensor.

Keywords: cellulose nanofibers, polypyrrole, conductive nanopaper, mechanical properties, electrical conductivity.

Graphical abstract

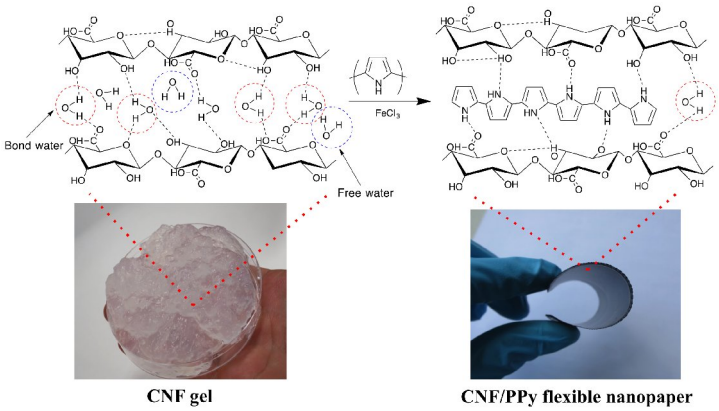

1. Introduction

The recent development of nanotechnology, together with the global concern for environment, is focusing on the use of bio-resources as alternative to mineral or non-renewable ones (Vijay Kumar Thakur, 2015). Nowadays, one exciting research area is the isolation and use of nanocelluloses. Cellulose is the most abundant biological raw material that can self-assemble into well-defined architectures at micro and nano scale. Therefore, from their origin, cellulose nanofibers are renewable, inexpensive, and non-toxic. In addition, and due to their chemical structure and high crystallinity, nanocelluloses have and remarkable physical, thermal, and mechanical properties, such as high specific surface area and high elastic modulus (Lavoine, Desloges, Dufresne, & Bras, 2012; Siró & Plackett, 2010). Among the different nanocelluloses, cellulose nanofibers (CNFs) consist of a long web-like structure with micrometer length and 10–100 nm in diameter that imparts unique properties. The isolation of CNFs can be performed by a wide variety of mechanical techniques such as refining, grinding, high pressure homogenization or cryocrushing (Wang, Sain, & Oksman, 2007). Different pre-treatments can also be applied to reduce the energy consumption as well as to modify the surface energy of CNFs (Jonoobi et al., 2015).

In combination with a suitable polymer matrix, cellulose nanofibers networks show considerable potential as effective reinforcement for high-quality bio-based composites. Likewise, their flexibility and high aspect ratio make CNFs outstanding materials for wide range of applications. The last decade, CNFs have been used as nanofillers to reinforce nanocomposites (Miao & Hamad, 2013; Saba et al., 2014) with thermoplastic and thermoset polymers for packaging products, construction materials, automobiles, furniture, and pharmaceuticals (Hoenich, 2006; Ioelovich, 2008; Jeon, Yang, & Kim, 2012; Kalia et al., 2011; Zhang et al., 2013). More recently, CNFs have gained much attention for its use as

biomedical material because of their exceptional surface chemistry and excellent biological properties (biocompatibility and biodegradability) (N. Lin & Dufresne, 2014).

Due to their benign nature, high available surface area, smoothness, and reduced porosity, CNF films have been reported as potential substrates for biosensors (Salas et al., 2014). However, and because of the intrinsic insulating characteristics, specific strategies need to be developed to impart electrical activity to CNF. In this sense, the combination of CNFs with conductive polymers (CPs) allows to extend the functionality of CNFs in energy storage devices, solar cells or electronic applications (Huang et al., 2013; Koga et al., 2014; Luo et al., 2014; Nyholm et al., 2011; Tammela et al., 2015; Wang et al., 2015; Zheng et al., 2013).

Conducting polymers are attractive candidates because they have good intrinsic conductivity, from a few to 500 S cm^{-1}. CPs are rendered conductive through a conjugated bond system along the polymer backbone. They are typically formed either through chemical oxidation or electrochemical oxidation of the monomer (Snook, Kao, & Best, 2011). In the chemical oxidation process, for example with iron chloride, the molecular weight and structural features of the resulting polymer are feasible to control. Among conducting polymers, polypyrrole (PPy) has an appreciable environmental stability (Buitrago-Sierra et al., 2013) and is easy to synthesize (Ansari, 2006; Eisazadeh et al., 2007; Huang et al., 2006; Trchova & Kova, 2003; Wang et al., 2001). PPy offers a greater degree of flexibility in electrochemical processing than most conducting polymers, and consequently the material has been the subject of much research as a supercapacitor or battery electrode (Snook et al., 2011). In 2006, Huang et *al.* investigated the *in-situ* polymerization of pyrrole on different pulp systems demonstrating the good adhesion between the conductive polymer and the fibers (Huang et al., 2006). The specific parameters and the sequence for the polymerization reaction, and their effect on the fiber degradation have also been studied (Beneventi, Alila, Boufi, Chaussy, & Nortier, 2006). Other authors have performed a soaking-polymerization

procedure on printing paper (Yuan et al., 2013). In this case, the conductive polymer remained mainly at the surface of the printing paper showing high value of surface electrical conductivity. The viability of coating PPy on CNF was demonstrated by Nyström et al., (2010). They verified the conductivity and the ion-charge capacity of a cellulose nanocomposite with high amount of PPy conductive polymer. In a further work, the authors investigated the mechanical properties of PPy-cellulose nancomposites of different porosity (Carlsson et al., 2012). In a different study (Nyström, Strømme, Sjödin, & Nyholm, 2012), they improved the capacitance of this type of cellulose nanocomposites. Later, Wang et al. (2015) performed surface modification of cellulose nanofibers to produce cellulose-based supercapacitors. The coating of PPy on CNF substrate has reduced moisture content of CNF in nature and also protected against degradation, as PPy is known to be insoluble in most solutions and solvents (Sasso et al., 2010). Carlsson et al. (2014) found that the individual nanocellulose fibrils should be coated by a thin layer of PPy less than 50 nm of thickness to avoid the problems associated with the low redox reaction rates and poor mechanical properties of nanocomposites.

In the present work, cellulose nanofibers are coated with polypyrrole using $FeCl_3$ as oxidant agent. In previous studies, large amounts of polypyrrole were used to obtain a substantial increase of the electrical activity of cellulose nanofibers. However, as consequence, brittle cellulose-nanocomposites were obtained. In this study, pyrrole was polymerized on cellulose nanofiber surface at certain reaction times to obtain very flexible and strong structures with electrical conductive capacity. The obtained CNF/PPy nanopapers were characterized considering their morphology and their mechanical, thermal and electrical response.

2. Materials and Methods

2.1 Materials

Bleached pine pulp from Arauco (Chile) was used as cellulose raw material. The cellulose content of the pulp was 95%. Pyrrole was supplied by Sigma Aldrich and used as received for the chemical synthesis of polypyrrole. The rest of materials, $FeCl_3$, Tween-80, 2,2,6,6-Tetramethyl-1-1-piperidinyloxy (TEMPO), sodium bromide (NaBr), sodium hypochlorite (NaOCl), HCl, NaOH, and NaCl were also supplied by Sigma Aldrich and used without further purification. Silver coating 3850 was supplied by Holland shielding system BV, Holland.

2.2 Preparation of CNF suspension

The bleached pine pulp (30 g dry weight) was dispersed in 2 L of distilled water and disintegrated at 6000 rpm for 30 min in a pulper (PAPEL QUIMIA, S.A, SPAIN). From this suspension, CNFs were extracted by means of a TEMPO-mediated oxidation followed by a mechanical homogenization (homogenizer NS1001L PANDA 2K-GEA, Italy). The TEMPO-mediated oxidation was performed at pH 10 (Fukuzumi et al., 2009) and the obtained cellulose suspension was diluted to 1wt% and passed through a high-pressure homogenizer, one time at 300 bars and three times at 600 bars of pressure. As a result, a transparent gel of cellulose nanofibers (CNF) at 1% concentration was obtained and stored at 4°C prior use.

2.3 Preparation of CNF and CNF/PPy nanopapers

CNF gel was first diluted to 0.2% with distilled water and dispersed by using a sonicator Q700 for 10 min (5 min pulse on, 2 min pulse off, and 5 min pulse on) at 60% of amplitude. Afterwards, the CNF suspension was filtered overnight using a glass filter funnel with a nitrocellulose membrane GSWP29325 (hydrophilic) of 0.22μm pore-size. After filtering, the nitrocellulose membrane was peeled off and the CNF cake was placed between two pieces of immobile transfer membranes of polyvinylidene fluoride (PVDF) (hydrophobic) of 0.45μm

pore-size to prevent adhesion between sample and membrane. Finally, the samples were dried using a laboratory sheet dryer at a vacuum pressure of -0.6 bar at 92 ± 3 °C for 20 min.

For the preparation of CNF/PPy nanopapers the same filtering procedure was used. Firstly, a dilute suspension of CNF (0.1%, 400 mg of dry weight) was sonicated for 10 min under the same setting conditions described above. This CNF suspension will be later mixed with a solution of pyrrole. For the preparation of the pyrrole solution, 0.1 mL of pyrrole was dissolved in 15 mL of 0.5 M HCl. After stirring the mixture for 3 min using magnetic stirrer, one drop (0.05 ml) of Tween-80 was added and stirred until completely homogenous. Afterwards, the solution of pyrrole was introduced into the above CNF suspension, and the mixture was stirred for 5 min. In order to initiate the polymerization, 0.578 g of $FeCl_3$ in 15 mL of HCl 0.5 M was added drop wise into the suspension. The final mixture was stirred at room temperature for 20, 40, 60, 120, and 180 min, in independent experiments, to get the different conductive nanopapers named as CNF/PPy20, CNF/PPy40, CNF/PPy60, CNF/PPy120, and CNF/PPy180, respectively. At the end, the mixture (CNF and PPy) was filtered using a glass filter and washed subsequently with 500 mL of 0.5 M HCl, 500 mL of 0.1 M NaCl, and 500 mL of distilled water. During the last washing with distilled water, the suspension was sonicated for 2 min to remove any small gas bubbles and to allow a better organization of CNF/PPy nanostructures without undesired side effects, such as crystal structure damage (Ali et al., 2014). Thereafter, the filtration was continued for 3 more hours until there is no residual water. The obtained CNF/PPy was finally dried in sheet dryer for 20 min.

2.4 Characterization of CNF and CNF/PPy nanopapers

The percentages of carbon, hydrogen, and nitrogen were determined by elemental analysis by means of a Perkin Elmer EA2400 series II. The measured amount of nitrogen was used to determine the PPy content in the formulation. The samples (3 mg) were pyrolyzed in helium

(He) at a combustion temperature of 925–930°C. Acetanilide powder (C_8H_9NO) was used as reference.

The FTIR spectrum of CNF/PPy nanopaper was obtain to characterize the absorption peaks of nanopapers after the chemical polymerization. For comparative purpose, FTIR spectra of pyrrole, cellulose nanofibers (CNF) and polypyrrole (PPy) were also recorded. The FTIR was performed using an ALPHA-FTIR spectrometer from Bruker, in the transmission mode in the range of 4000–500 cm^{-1} using 24 scans.

Mechanical properties of nanocomposites were evaluated using tensile test under control conditions of 50% relative humidity at room temperature. The rectangle specimens of CNF nanopaper (50×5×0.055) mm and CNF/PPy nanopapers (50×5×(0.07±0.015)) mm were tested using a Universal Testing Machine HOUNSFIELD, equipped with a 250 N load cell with a cross-head speed of 5 mm/min. These parameters were set according to previous work (Hamedi et al., 2014). Data of at least five specimens were collected to obtain the statistical standard deviation for each sample.

The cross section surfaces of CNF and CNF/PPy nanopapers, as well as the PPy platelet, were observed under a field emission scanning electron microscope (FE-SEM) HITACHI S-4100. The samples from tensile test were coated with gold using a sputter. The images were taken using secondary electron detector at 20 kV accelerating voltage for PPy powder and 12 kV for CNF and CNF/PPy nanopapers to prevent burning the samples.

Dynamic mechanical analysis (DMA) was employed to study the viscoelastic behaviour of CNF and CNF/PPy nanopapers with the changing of temperature, using a DMA/SDTA861e instrument from Mettler Toledo, operating in 3 point bending mode. The isochronal scans were recorded from -100 to 200°C at a heating rate of 5°C min^{-1}, at 1Hz of frequency and 15 µm of amplitude. The sample dimensions were (5×20×(0.07±0.015)) mm. A reducing force mode was engaged by regulating the static force during the test to minimize creep. The

experiment was performed under dry nitrogen (N_2) flow to limit water sorption during experiment.

Thermogravimetric analysis (TGA) was used to determine the lost weight with the temperature and the degradation temperatures of CNF/PPy nanopapers. The samples were heated from 30 to 600°C at the heating rate of 10°C min^{-1} using a METTLER TOLEDO ultra micro balance, TGA/DSC. The purge gas was nitrogen with a flowing rate of 40 mL/min.

The electrical conductivity of the obtained nanopapers was determined based on the measurement of the resistance (R) over the length of the specimens using an Agilent 34461A digital multimeter. All CNF/PPy nanopapers were cut into (5×20×(0.075 ± 0.015)) mm stripes. Silver paint was applied at room temperature at the end of both sides of each sample to ensure good electrical contact with the clip probes. The measurement was done 16 h after the application of silver paint. The conductivity was calculated by equation: $\sigma = (L/R \times w \times d)$, where L, w, and d are length, width, and thickness of the sample, respectively.

Cyclic voltammetry (CV) was carried out with a standard three-electrode electrochemical cell (working electrode), a platinum wire (counter electrode), and a 2 M NaCl-saturated Ag/AgCl electrode (reference electrode) by using a Potentistat/Galvanostat Model 273A Princeton equipment. Cyclic voltammograms were recorded in the potential window of −0.9 to +0.9 V vs Ag/AgCl at different scan rate of 5, 20, 50, 100, and 200 mV $s^{-}1$. CView and originPro software were used to plot the graphs. The sample dimensions were (7×15×(0.075±0.015)) mm. The capacitance and specific capacitance were calculated by $C_{sp} = i/(m.v.\Delta V)$, where C_{sp} (F g^{-1}) is the specific capacitance, i is the integration in CV curve, v is the scan rate in mV s^{-1}, m is the mass (g) of electrode material, and ΔV is the potential difference window ΔV = 1.8 V.

3. Results and discussion

Scheme 1 illustrates the intermolecular interaction between CNF chains, and the interaction mechanism between CNF and PPy after the in situ chemical polymerization using $FeCl_3$ as oxidant agent; pictures of CNF gel (**Sc. 1a**), high transparent CNF nanopaper (**Sc. 1b**), CNF/PPy nanopaper (**Sc. 1c**), as well as the high flexibility of CNF/PPy nanopapers (**Sc. 1d**) are also depicted in scheme 1. The obtained CNF/PPy nanopapers were flexible black films due to the presence of black precipitated PPy on CNF surface. The yield of PPy (%) at each reaction time is presented in the supplementary information **S1**. Likewise, the thickness, density and porosity of each sample are listed in **S3**.

Sc. 1 Interaction between CNF and PPy, and photographs of CNF gel (a), CNF nanopaper (b), CNF/PPy (c), and flexible CNF/PPy nanopaper (d).

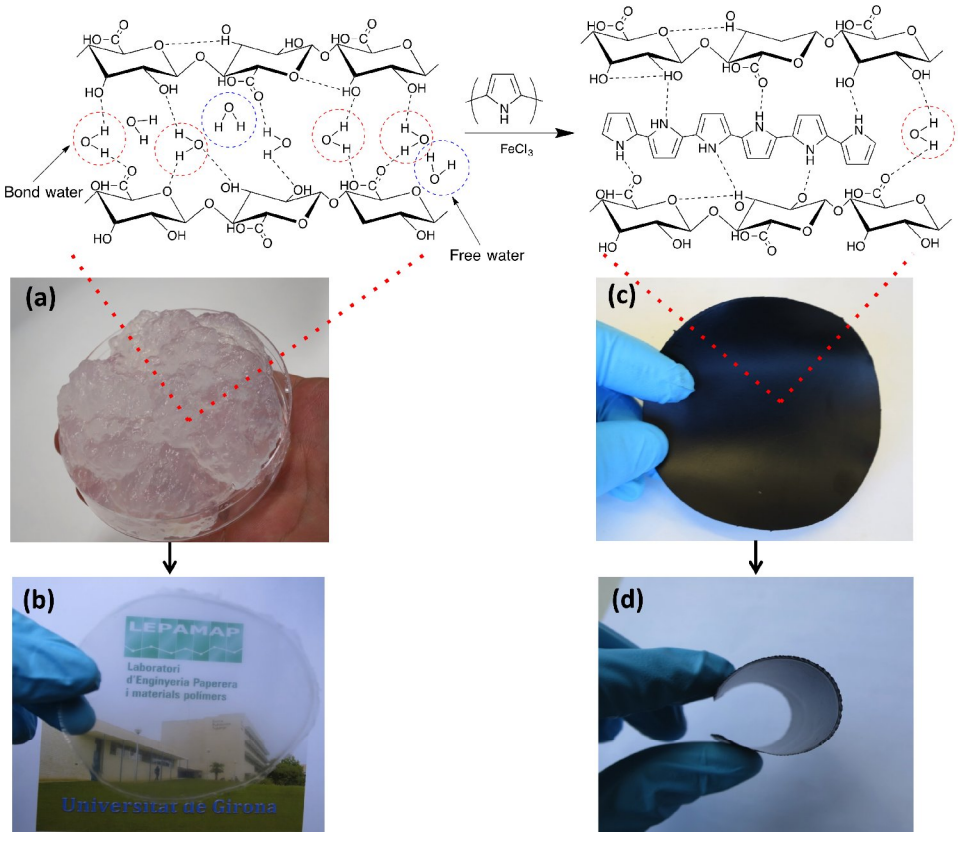

The FTIR absorption spectrum of CNF/PPy nanopaper is shown in **Fig. 1**. For comparison, FTIR spectra of cellulose nanofibers (CNF), pyrrole, and polypyrrole are presented in **S4**. CNF/PPy60 nanopaper exhibited similar spectrum as polypyrrole but with all the major peaks shifted to lower wave number, which supports the existing interaction between –N–H of PPy and C–OH of CNF by means of hydrogen bonding (Firoz Babu et al., 2012). The band at 1707 cm^{-1} is assigned to the C=O bond of carboxylic acid group of CNF in the CNF/PPy nanopaper. Comparing this wavelength with the carboxyl group one of CNF (**S4b**), the absorption peak has shifted towards higher values, which is representative of the interaction between CNF and the coating PPy. The strong band at 1546 cm^{-1} is characteristic of the C=C stretching of the aromatic ring of PPy. The absorption peaks at 1306 cm^{-1}, 1017 cm^{-1}, and 888 cm^{-1} are assigned to the C–N stretching, C–H stretching and N–H wagging of the polypyrrole ring, respectively. In the region 1300-800 cm^{-1} the absorption peaks corresponding to C–H bending and C-O ethers links for the CNF are also found (see **S4**).

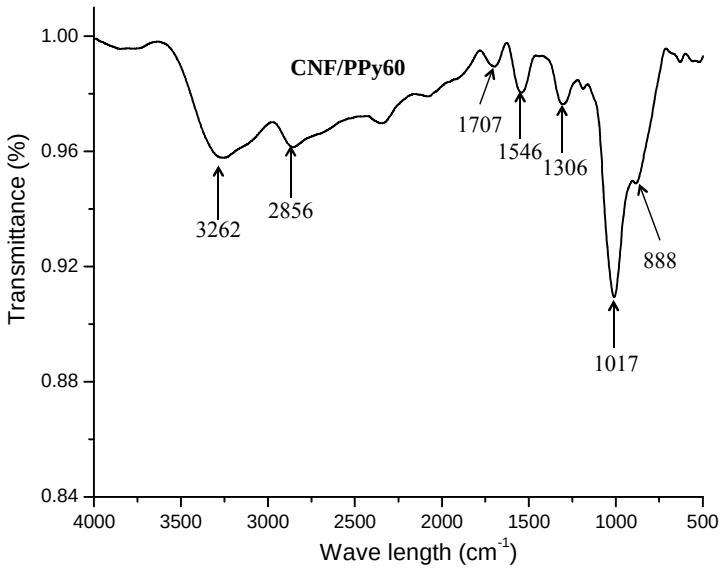

Fig. 1 FT-IR spectrum CNF/PPy60 nanopaper.

The stress-strain curves, tensile strength and Young's modulus of neat CNF and CNF/PPy nanopapers are presented in **Fig. 2**. CNF nanopaper exhibited outstanding tensile strength of

224 MPa and Young's modulus of 14.5 GPa. These values are higher than previous works (González et al., 2014; Sehaqui et al., 2010), where the nanopapers were produced by means of Rapid Köthen (sheet dryer). These high mechanical properties are related to the strong interactions between nanofibrils and to the nanofibril entanglements (Boufi et al., 2014); some nanofibrils alignment is also expected during the filtration procedure. The sonication step introduced in our methodology helped to remove the possible voids between nanofibrils and provided a homogeneous structure resulting in a low porosity of the final nanopaper, as presented in **S2** and **S3**. Moreover, CNFs from TEMPO mediated oxidation show high nanofibrillation degree and unchanged original crystallinity (Isogai et al., 2011), which is responsible of the high mechanical properties of the obtained CNF nanopaper. However, the tensile strength and Young's modulus of CNF/PPy20 decreased to 124 MPa and 8.9 GPa, respectively, and continued to decrease until 94 MPa and 8.8 GPa, respectively, for the CNF/PPy180 nanopaper. Therefore, the incorporation of PPy in the structure produced a reduction in the mechanical properties of the unmodified CNF, with a maximum decrease of 58% for the tensile strength and of 39% for the Young's modulus (CNF/PPy180). As a result, CNF/PPy nanopapers were more brittle than neat CNF nanopaper. The elongation at break also decreased with the incorporation of PPy, from 3.5% for CNF to 1.55% for CNF/PPy180. It is expected that the PPy coated on CNF surface lessened the number of CNF inter-fibril –OH interactions, as the –NH group of pyrrole interacted with the hydroxyl groups of cellulose nanofibrils. The coating of CNF with PPy increased the porosity from 10.45% (CNF) to 19.45 % (CNF/PPy180) as shown in **S3**. The higher porosity caused the premature breaking point of the CNF/PPy nanopapers, showing the decrease in their final tensile strength. In addition, the PPy-coated CNF had fewer CNF interfibrils connections that were responsible of the diminution in the rigidity of the PPy-modified CNF nanopapers. However, CNF/PPy nanopapers still showed considerably high mechanical properties. Moreover, after certain

level of PPy coating (after 40 minutes of reaction time), the strength and the modulus were not very much reduced. Instead, higher content of PPy kept lessening the toughness of the resulting CNF/PPy nanopaper. It is worth mentioning, however, that all CNF/PPy nanopaper showed great flexibility (**Sc. 1d**) together with these remarkable mechanical properties. The values of the mechanical properties with the thickness, density and porosity of each nanopaper are presented in **S3**.

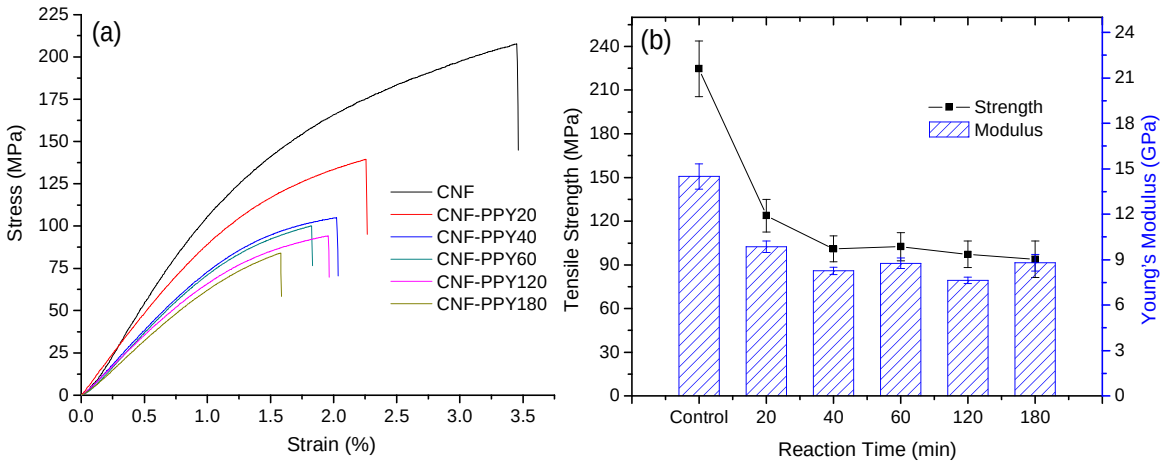

Fig. 2 (a) Stress–strain curves and (b) Tensile strength and Young's modulus of CNF and CNF/PPy nanopapers at different reaction times.

To support this, the fracture surfaces of CNF and CNF/PPy nanopapers were observed by FE-SEM (**Fig. 3)**. FE-SEM microphotograph of PPy platelet is shown in **Fig. 3a**. PPy tends to agglomerate itself due to strong intermolecular interactions. CNF nanopaper showed a compact multilayer configuration of interconnected cellulose nanofibers **(Fig. 3b)**. This multilayer structure and tight connection between layers contributed to the high mechanical performance of the ensuing pure CNF nanopaper. The multilayer structure was conserved for the PPy-coated CNF nanopaper **(Fig. 3c)**. With the addition of PPy the surface roughness of CNF/PPy nanopaper increased, as the PPy platelets interpenetrated the cellulose nanofibers

network. The perfect distribution of PPy within the cellulose nanofiber network is evidenced in **Fig. 3d**. However, the coating of excess PPy on the CNF surface induced higher roughness, as shown in **Fig. 3e**. This leaded to a diminish in the mechanical properties because PPy-PPy-bonds has low mechanical properties and the PPy coating reduced the number of CNF-CNF strong bonds (Nyström et al., 2010).

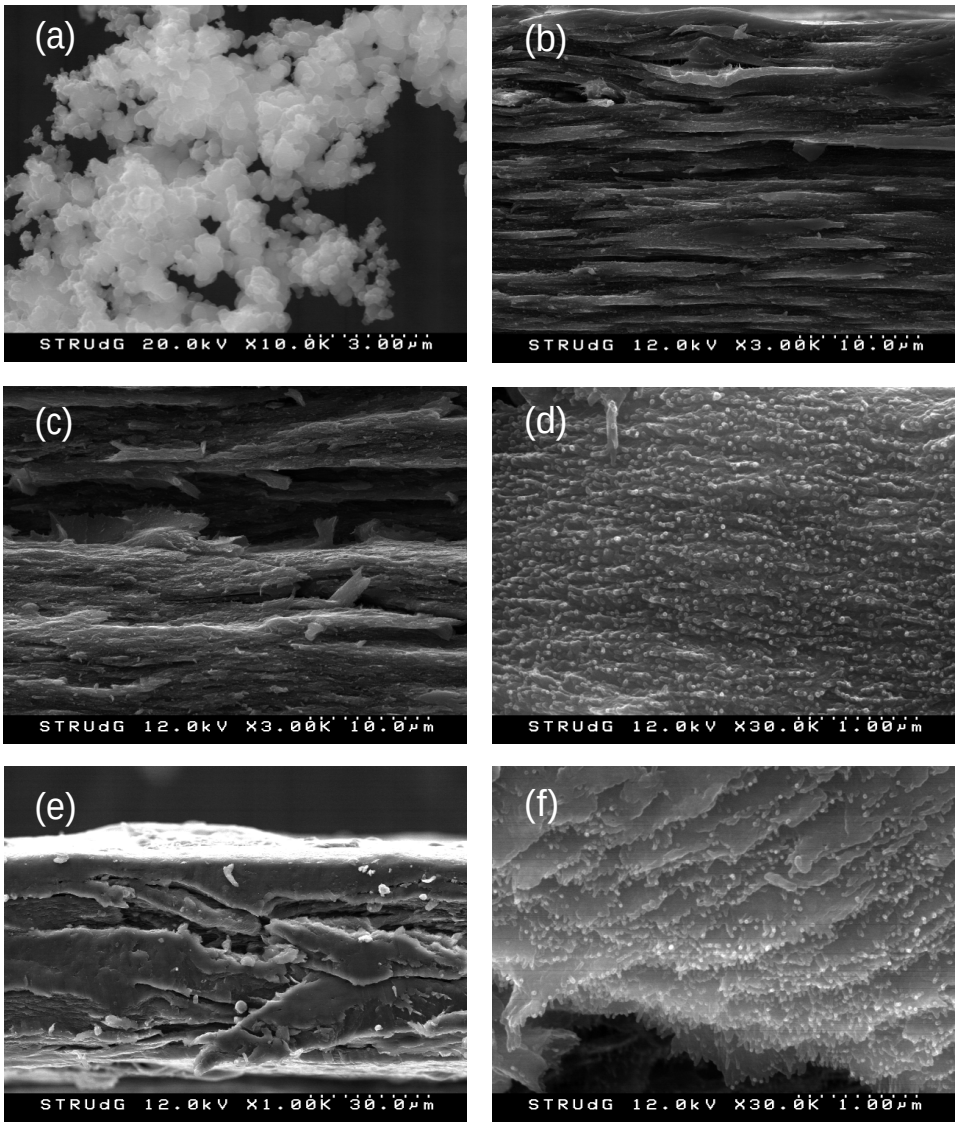

Fig. 3 FE-SEM of (a) PPy platelet; (b) cross-sectional surface of CNF nanopaper; (c-d) CNF/PPy20 nanopaper at magnification of 3000X and 30 000X and (e-f) CNF/PPy120 nanopaper at 1000X and 30000X.

The PPy-PPy interactions are intrinsically weaker than cellulose-cellulose ones (Zhang et al, 2013) and PPy itself possesses scarce mechanical properties (Sasso et al., 2010). Moreover, the tensile force was applied to parallel layers of CNFs and PPy, resulting in a more brittle nanopaper than the neat CNF nanopaper (Sasso et al., 2010). The microstructure of CNFs (**Fig. 3b**) shows their fibrils alignment and smoothness at the breaking point. The fibrils were bonded together leading to a strong interface that undergoes to CNF nanopaper with very high mechanical strength. With an excess of polypyrrole on CNF surface (**Fig. 3f)** all CNFs chains were coated and residual PPy platelet was found, confirming that during the polymerization reaction, not all polypyrrole (–NH) interacted with cellulose nanofibers (–OH).

The thermal mechanical properties of three materials namely neat CNF nanopaper, CNF/PPy20 and CNF/PPy120 nanopapers were studied by DMA. In the test, an oscillating force is applied to a sample and the material's response is analysed. The data presented in **Fig. 4** corresponds to the complex modulus (E*=E'+iE''). The complex modulus is composed of real and imaginary terms, equivalent to the storage modulus (E') and loss modulus (E''), respectively. The materials obtained in the present study exhibited mainly an elastic behaviour, with values for storage modulus much higher than the ones for loss modulus (E'>>E''), so then the complex modulus is very similar to the storage modulus (E*≈E') (**S5**). The dynamo-mechanic test started at -100ºC of temperature. Under conditions of low molecular mobility, cellulose composites can be very stiff (Sehaqui et al., 2011) and, as expected, the modulus decreases with increasing temperature. The complex modulus of our pure CNF nanopaper, at this low temperature, was above 25 GPa and decreased with

temperature. The value of the storage modulus indicates how elastic the material is, and ideally would be equivalent to Young's modulus at room temperature. In our case, the complex modulus at 23°C for CNF, CNF/PPy20, and CNF/PPy120 nanopapers were 15.3, 10.9, and 7.8 GPa, while the Young's modulus from tensile test were 14.5, 9.8, and 8.8 GPa, respectively. This difference can be explained for the experimental methods in determining each value. Young's modulus is calculated from the slope of a line over a range of stresses and strains, whereas the complex modulus (or storage modulus) comes from what can be considered a point on the line. Moreover, the tests methods are very different as one material is constantly stretched in the stress-strain tests, whereas it is oscillated under bending conditions in the dynamic test (Int, 2008). For CNF nanopaper, molecules of cellulose are tightly compressed at -77°C temperature and at -60°C temperature for CNF/PPy, which define the solid-state transition in each case (Int, 2008). When the materials are heated up, localized movements and solid chain movements occurred. This represents the gamma transition (Tγ) that involves association with water as cellulose contains some moisture (Int, 2008; Sehaqui et al., 2011). As heating continued, a glass transition was not found for all samples; the native CNFs has no glass transition because of its high degree of crystallinity (Rastogi et al., 2014). The complex modulus of CNF nanopaper steady diminished with the temperature between 40°C and 160°C due to a slippage of crystallites between one another. Conversely, the presence of PPy on CNF surface hindered chain movements making CNF/PPy slowly changed from glassy to rubbery state compared to CNF nanopaper. At the temperature between 40 and 110°C, CNF/PPy showed the region of rubbery plateau, which is related to physical and chemical cross-link between PPy and CNF chains (Henriksson et al., 2011). Moreover, above 160°C, PPy-modified nanopapers showed higher complex modulus than pure CNF nanopaper, telling that PPy improved thermal stability of nanopapers.

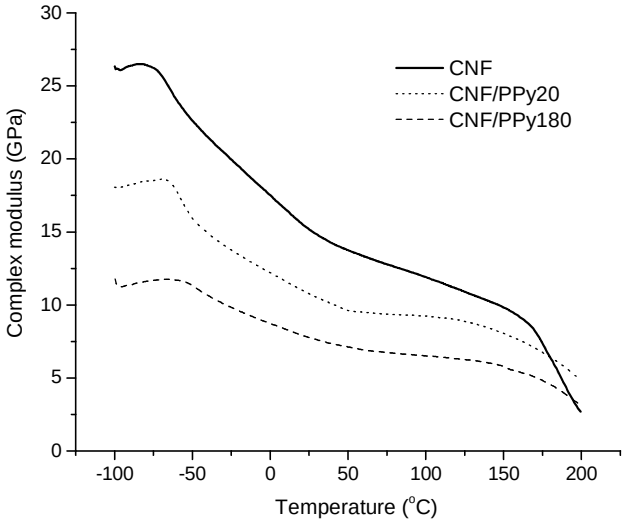

Fig. 4 Complex modulus of CNF and CNF/PPy nanopapers at frequency of 1Hz.

The degradation temperatures of CNF, PPy, and CNF/PPy nanopapers were studied by thermogravimetric analysis (**Fig. 5a**). The initial weight loss of about 7% in the range of 50–105°C was due to residual moisture present in the samples (Lee et al., 2012). In CNF nanopaper, cellulose pyrolysis started at 201°C and continued until around 330°C leading to depolymerization of solid cellulose to form active cellulose and thereafter various anhydro-monosaccharides, retroaldol, dehydrated species, carbon oxides, and char (Lin et al., 2009; Nyström et al., 2010). The weight loss for CNF nanopaper was of 61.5% at 330°C and of 73% at 600°C, similar to the values found in previous studies (Nyström et al., 2010). In the case of CNF/PPy180 nanopaper, the weight loss between 230°C and 350°C was of 31% and of 61.5% at 600°C. For this nanopaper, the loss was not only a result of the degradation process of the cellulose but also partly because of the thermal degradation of the polymer backbone in polypyrrole. For the polymer itself (PPy), the total weight loss at 600 °C was 42%, following a slow degradation mechanism. One can say that the degradation kinetics of PPy is much slower than the degradation of CNF. PPy degrades in two steps, a degradation process involving the counterions first and the polymer backbone degradation afterwards.

The process during which the counterion is expelled occurs before the polymer backbone degradation in PPy and is probably responsible for shifting the main degradation of CNF/PPy to have its maximum degradation temperature at a lower temperature than the one for CNF (Nyström et al., 2010). The values of the maximum degradation temperatures can be seen from the derivative thermogravimetric curves **(Fig. 5b)**. The thermal degradation of CNF from TEMPO-oxidation was broad and consisted of mainly two peaks around 232°C and 296°C, both below the degradation point of original cellulose (~310°C). This confirms the formation of sodium carboxylate groups at the C_6 primary hydroxyls of cellulose. According to literature (Fukuzumi, 2012), the first degradation peak corresponds to the degradation of sodium anhydroglucuronate units, and the second relates to the degradation of cellulose chains containing more unstable anhydroglucuronate units in the crystal surface. The decomposition of PPy was found at 230°C; therefore, CNF nanopaper with higher amount of PPy showed a decrease in the degradation temperature of the CNF/PPy nanopaper (decomposition temperature of 286°C for CNF/PPy20 and of 257°C for CNF/PPy180) **(Fig. 5b)**. The morphology and stability of PPy depend on its composition. Conducting films made with ferric chloride have chloride counterions (dopant), which has a higher mobility than other counterions (Saville, 2005). From the TGA/DTG analysis, it is important to note that PPy coated on cellulose nanofibers decreased the maximum degradation temperature and it slowed the kinetics of the degradation mechanism of the resulting CNF/PPy nanopaper.

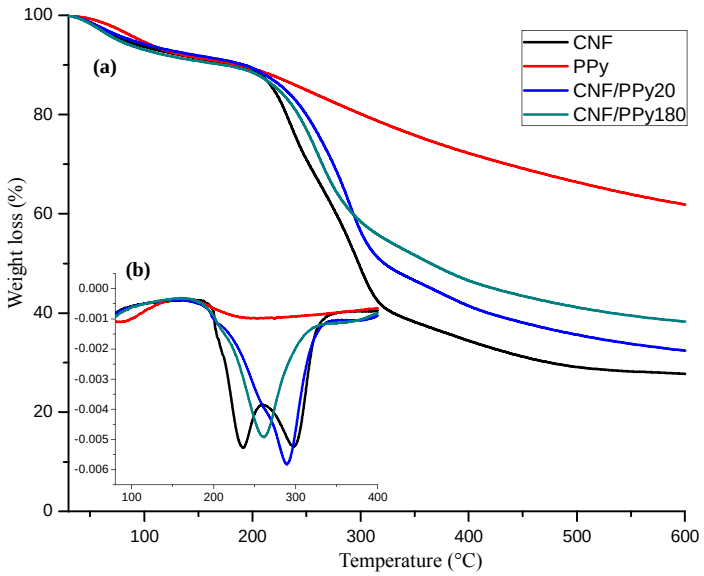

Fig. 5 TGA (a) and DTG (b) of pure CNF nanopaper and CNF/PPy nanopapers as a function of temperature.

The electrical conductivities, together with the results of elemental analysis, are shown in **Fig. 6**. In situ chemical polymerization of PPy on CNF substrate enhanced electrical properties of CNF. Elemental analysis confirmed the higher amount of PPy on CNF nanofibers with increasing the reaction time. The electrical conductivities of nanopapers depend on the amount of coated PPy. From the results, the electrical conductivity of CNF/PPy20 was 10^{-5} S·cm^{-1}, which is already similar to that of silicon (1.5 10^{-5} S·cm^{-1}), and reached up to 5.2 10^{-2} S·cm^{-1} for the CNF/PPy180 nanopaper, at the level of other semiconductors. Considering the insulating property of cellulose nanofibers (between 10^{-13}–10^{-8} S·cm^{-1}, depending on moisture content), the addition of a very low content of PPy filler (only 8%) turned the PPy-modified CNF nanopapers in a semi-conductor material, thanks to the uniformly connected conductive networks on cellulose nanofibers surface during the filtering and drying process (Koga et al., 2014). The amount of polypyrrole in the nanopaper steadily increased with the reaction, whereas the conductivity improved dramatically. The

electrical conductivity was enlarged 2 orders of magnitude with only 18% of PPy, and one more order of magnitude above with only 20% PPy. The increase in porosity leads to a better-bonded structure, resulting in higher electrical conductivity (**S3**).

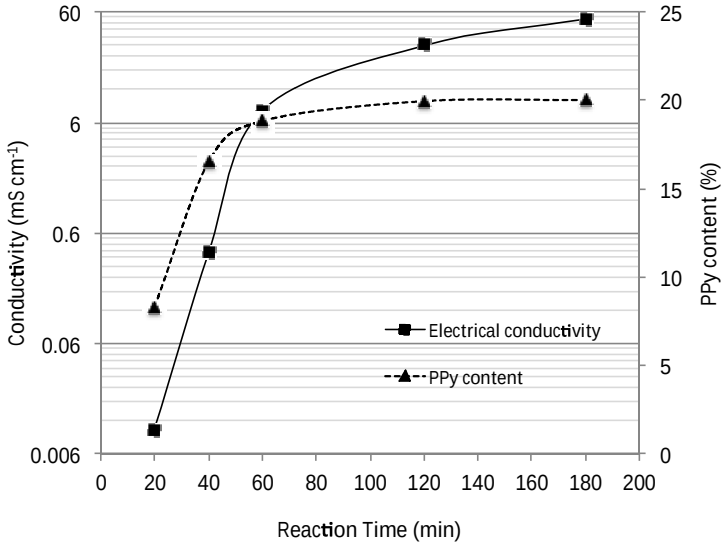

Fig. 6 Electrical conductivity and PPy content in CNF/PPy nanopapers with the different reaction time.

The electrochemical properties of the conducting CNF/PPy180 were determined by cyclic voltammetry in 2 M NaCl electrolyte. **Fig. 7** depicts different scan rate of 5, 20, 50, 100, and 200 mV s^{-1} of CNF/PPy180 in the potential window between -0.9 and +0.9 V (vs. Ag/AgCl). All the curves are elliptical, with increased current upon increasing the scan rate. The oxidation and reduction peaks did not appear due to the relatively small amount of pyrrole (20%) in the nanopapers. The specific capacitance found for CNF/PPy180 at 5 mV s^{-1} was 7.40 F g^{-1}, which decreased to 0.35 F g^{-1} at the highest scan rate of 200 mV s^{-1}. The dramatic decrement of specific capacitance has been related to the sample compression during the sheet drying, which reduced the porosity. When the porosity is decreased the ion mass transport is too slow to allow for full utilization of the inherent charge storage capacity for

scan rates above 5mV s^{-1} (Wang 2014). As mentioned by Carlsson et al., (2012), porous samples allow fast transport of anions throughout the electro-active material. They found that the capacity of compact samples decreased with increasing scan rate while the porous samples showed a slight increase in capacity.

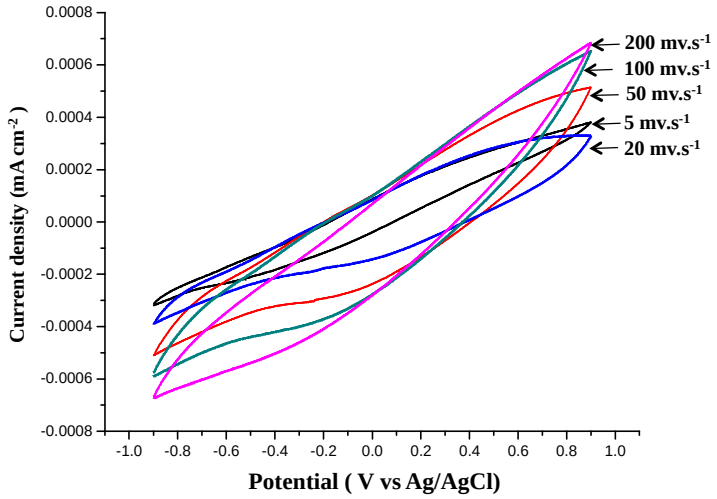

Fig. 7 Cyclic voltammograms of CNF/PPy180 at different scan rate of 5, 20, 50, 100, and 200 mV s^{-1}.

4. Conclusions

A strong and electrically conductive nanopaper was obtained by coating softwood cellulose nanofibers with polypyrrole. The structure of PPy modified nanopapers were composed of multilayers of CNF with PPy chains interpenetrating the cellulose nanofiber network. The obtained pure CNF nanopaper had very high tensile properties, with 224 MPa of strength and 14.5 GPa of elastic modulus. On the other hand, nanopapers containing up to 20% of PPy showed lower but still good mechanical properties (94 MPa strength and 8.8 GPa modulus), with an electrical conductivity of 5.2 10^{-2} S cm^{-1}. In fact, the conductivity of this PPy-modified CNF nanopaper was three orders of magnitude above the one of typical semiconductor like silicon (1.5 10^{-5} S cm^{-1}). This modification changed the nature of CNF

nanopaper from insulator to semiconductor material, after coating with polypyrrole polymer. Compared to previous results in the literature, the proposed methods and products provided strong and flexible cellulose nanopapers of high mechanical properties and the electrical conductivity in the range of semiconductors. With these results, new applications can be expected for cellulose nanofibers as biodegradable thin-film transistors or as biosensors. This work opens the door to use cellulose nanofibers in green, low-cost, and portable electronic devices in the future.

5. Acknowledgements

The authors want to thank the financial support of the European Commission (Erasmus Mundus Project Techno II, ref. 372228-1-2012-1-FR-ERA MUNDUS-EMA21).

References

Ali, F., Reinert, L., Levêque, J.-M., Duclaux, L., Muller, F., Saeed, S., & Shah, S. S. (2014). Effect of sonication conditions: Solvent, time, temperature and reactor type on the preparation of micron sized vermiculite particles. *Ultrasonics Sonochemistry*, *21*(3), 1002–1009.

Ansari, R. (2006). Polypyrrole Conducting Electroactive Polymers: Synthesis and Stability Studies. *E-Journal of Chemistry*, *3*(4), 186–201.

Beneventi, D., Alila, S., Boufi, S., Chaussy, D., & Nortier, P. (2006). Polymerization of pyrrole on cellulose fibres using a FeCl3 impregnation- pyrrole polymerization sequence. *Cellulose*, *13*(6), 725–734.

Boufi, S., Kaddami, H., & Dufresne, A. (2014). Mechanical Performance and Transparency of Nanocellulose Reinforced Polymer Nanocomposites. *Macromolecular Materials and Engineering*, *299*(5), 560–568.

Buitrago-Sierra, R., García-Fernández, M. J., Pastor-Blas, M. M., & Sepúlveda-Escribano, A. (2013). Environmentally friendly reduction of a platinum catalyst precursor supported on polypyrrole. *Green Chemistry*, *15*(7), 1981–1990.

Carlsson, D. O., Mihranyan, A., Strømme, M., & Nyholm, L. (2014). Tailoring porosities and electrochemical properties of composites composed of microfibrillated cellulose and polypyrrole. *RSC Advances*, *4*(17), 8489 – 8497.

Carlsson, D. O., Nyström, G., Zhou, Q., Berglund, L. A., Nyholm, L., & Strømme, M. (2012). Electroactive nanofibrillated cellulose aerogel composites with tunable structural and electrochemical properties. *Journal of Materials Chemistry*, *22*(36), 19014–19024.

Eisazadeh, H., Engineering, C., & Box, P. O. (2007). Studying the Characteristics of Polypyrrole and its Composites. *World Journal of Chemistry*, *2*(2), 67–74.

Firoz Babu, K., Dhandapani, P., Maruthamuthu, S., & Anbu Kulandainathan, M. (2012). One pot synthesis of polypyrrole silver nanocomposite on cotton fabrics for multifunctional property. *Carbohydrate Polymers*, *90*(4), 1557–1563.

Fukuzumi, H. (2012). *Studies on structures and properties of TEMPO-oxidized cellulose nanofibril films*. University of Tokyo, Japan.

Fukuzumi, H., Saito, T., Iwata, T., Kumamoto, Y., & Isogai, A. (2009). Transparent and high gas barrier films of cellulose nanofibers prepared by TEMPO-mediated oxidation. *Biomacromolecules*, *10*(1), 162–165.

González, I., Alcalà, M., Chinga-Carrasco, G., Vilaseca, F., Boufi, S., & Mutjé, P. (2014). From paper to nanopaper: Evolution of mechanical and physical properties. *Cellulose*, *21*(4), 2599–2609.

Hamedi, M. M., Hajian, A., Fall, A. B., Hkansson, K., Salajkova, M., Lundell, F., … Berglund, L. a. (2014). Highly conducting, strong nanocomposites based on nanocellulose-assisted aqueous dispersions of single-wall carbon nanotubes. *ACS Nano*, *8*(3), 2467–2476.

Henriksson, M., Fogelström, L., Berglund, L. a., Johansson, M., & Hult, A. (2011). Novel nanocomposite concept based on cross-linking of hyperbranched polymers in reactive cellulose nanopaper templates. *Composites Science and Technology*, *71*(1), 13–17.

Hoenich, N. (2006). Cellulose for medical applications: past, present, and future. *BioResources*, *1*(2), 270–280.

Huang, B., Kang, G. J., & Ni, Y. (2006). Preparation of conductive paper by in-situ polymerization of pyrrole in a pulp fibre system. *Conductive Papers*, *2*, 38–42.

Huang, J., Zhu, H., Chen, Y., Preston, C., Rohrbach, K., Cumings, J., & Hu, L. (2013). Highly transparent and flexible nanopaper transistors. *ACS Nano*, *7*(3), 2106–2113.

Int, H. P. M. (2008). *Dynamic Mechanical Analysis: A Practical Introduction. Textbook*. New york: CRC Press.

Ioelovich, M. (2008). Cellulose as a nanostructured polymer: A short review. *BioResources*, *3*(4), 1403–1418.

Isogai, A., Saito, T., & Fukuzumi, H. (2011). TEMPO-oxidized cellulose nanofibers. *Nanoscale*, *3*(1), 71–85.

Jeon, G., Yang, S. Y., & Kim, J. K. (2012). Functional nanoporous membranes for drug delivery. *Journal of Materials Chemistry*, *22*, 14814 – 14834.

Jonoobi, M., Oladi, R., Davoudpour, Y., Oksman, K., Dufresne, A., Hamzeh, Y., & Davoodi, R. (2015). Different preparation methods and properties of nanostructured cellulose from various natural resources and residues: a review. *Cellulose*, *22*(2), 935–969.

Kalia, S., Dufresne, A., Cherian, B. M., Kaith, B. S., Avérous, L., Njuguna, J., & Nassiopoulos, E. (2011). Cellulose-based bio- and nanocomposites: A review. *International Journal of Polymer Science*, *2011*, 1 – 35.

Koga, H., Nogi, M., Komoda, N., Nge, T. T., Sugahara, T., & Suganuma, K. (2014). Uniformly connected conductive networks on cellulose nanofiber paper for transparent paper electronics. *NPG Asia Materials*, *6*, 1–8.

Lavoine, N., Desloges, I., Dufresne, A., & Bras, J. (2012). Microfibrillated cellulose - its barrier properties and applications in cellulosic materials: a review. *Carbohydrate Polymers*, *90*(2), 735–64.

Lee, K. Y., Tammelin, T., Schulfter, K., Kiiskinen, H., Samela, J., & Bismarck, A. (2012). High performance cellulose nanocomposites: Comparing the reinforcing ability of bacterial cellulose and nanofibrillated cellulose. *ACS Applied Materials and Interfaces*, *4*(8), 4078–4086.

Lin, N., & Dufresne, A. (2014). Nanocellulose in biomedicine : Current status and future prospect. *European Polymer Journal*, *59*, 302–325.

Lin, Y., Cho, J., Tompsett, G. a, Westmoreland, P. R., & Huber, G. W. (2009). Kinetics and Mechanism of Cellulose Pyrolysis. *Physical Chemistry*, *113*(January), 20097–20107.

Luo, Y., Zhang, J., Li, X., Liao, C., & Li, X. (2014). The Cellulose Nanofibers for Optoelectronic Conversion and Energy Storage. *Journal of Nanomaterials*, *2014*, 1–13.

Miao, C., & Hamad, W. Y. (2013). Cellulose reinforced polymer composites and nanocomposites : a critical review. *Cellulose*, *20*, 2221–2262.

Nyholm, L., Nyström, G., Mihranyan, A., & Strømme, M. (2011). Toward Flexible Polymer and Paper-Based Energy Storage Devices. *Advanced Materials*, *23*, 3751–3769.

Nyström, G., Mihranyan, A., Razaq, A., Lindström, T., Nyholm, L., & Strømme, M. (2010). A nanocellulose polypyrrole composite based on microfibrillated cellulose from wood. *The Journal of Physical Chemistry. B*, *114*(12), 4178–4182.

Nyström, G., Strømme, M., Sjödin, M., & Nyholm, L. (2012). Rapid potential step charging of paper-based polypyrrole energy storage devices. *Electrochimica Acta*, *70*, 91–97.

Rastogi, V., Stanssens, D., & Samyn, P. (2014). Mechanism for Tuning the Hydrophobicity of Microfibrillated Cellulose Films by Controlled Thermal Release of Encapsulated Wax. *Materials*, *7*(11), 7196–7216.

Saba, N., Tahir, P., & Jawaid, M. (2014). A Review on Potentiality of Nano Filler/Natural Fiber Filled Polymer Hybrid Composites. *Polymers*, *6*, 2247–2273.

Salas, C., Nypelö, T., Rodriguez-Abreu, C., Carrillo, C., & Rojas, O. J. (2014). Nanocellulose properties and applications in colloids and interfaces. *Current Opinion in Colloid and Interface Science*, *19*(5), 383–396.

Sasso, C., Zeno, E., Petit-Conil, M., Chaussy, D., Belgacem, M. N., Tapin-Lingua, S., & Beneventi, D. (2010). Highly Conducting Polypyrrole/Cellulose Nanocomposite Films with Enhanced Mechanical Properties. *Macromolecular Materials and Engineering*, *295*(10), 934–941.

Saville, P. (2005). *Polypyrrole Formation and Use*. *DRDC Atlantic TM, Canada* (Vol. 004).

Sehaqui, H., Allais, M., Zhou, Q., & Berglund, L. a. (2011). Wood cellulose biocomposites with fibrous structures at micro- and nanoscale. *Composites Science and Technology*, *71*(3), 382–387.

Sehaqui, H., Liu, A., Zhou, Q., & Berglund, L. A. (2010). Fast preparation procedure for large, flat cellulose and cellulose/inorganic nanopaper structures. *Biomacromolecules*, *11*(9), 2195–2198.

Siró, I., & Plackett, D. (2010). Microfibrillated cellulose and new nanocomposite materials: a review. *Cellulose*, *17*(3), 459–494.

Snook, G. a., Kao, P., & Best, A. S. (2011). Conducting-polymer-based supercapacitor devices and electrodes. *Journal of Power Sources*, *196*(1), 1–12.

Tammela, P., Wang, Z., Frykstrand, S., Zhang, P., Sintorn, I.-M., Nyholm, L., & Strømme, M. (2015). Asymmetric supercapacitors based on carbon nanofibre and polypyrrole/nanocellulose composite electrodes. *RSC Adv.*, *5*(21), 16405–16413.

Trchova, M., & Kova, J. (2003). Synthesis and structural study of polypyrroles prepared in the presence of surfactants. *Synthetic Metals*, *138*, 447–455.

Vijay Kumar Thakur. (2015). *Nanocellulose Polymer Nanocomposites: Fundamentals and Applications*. MA: Wiley.

Wang, B., Sain, M., & Oksman, K. (2007). Study of structural morphology of hemp fiber from the micro to the nanoscale. *Applied Composite Materials*, *14*(2), 89–103.

Wang, L.-X., Li, X.-G., & Yang, Y.-L. (2001). Preparation, properties and applications of polypyrroles. *Reactive and Functional Polymers*, *47*, 125–139.

Wang, Z., Carlsson, D. O., Tammela, P., Hua, K., Zhang, P., Nyholm, L., & Strømme, M. (2015). Surface Modified Nanocellulose Fibers Yield Conducting Polymer-Based Flexible Supercapacitors with Enhanced Capacitances. *ACS Nano*, *9*(7), 7563–7571.

Wang, Z., Tammela, P., Zhang, P., Strømme, M., & Nyholm, L. (2014). Efficient high active mass paper-based energy-storage devices containing free-standing additive-less polypyrrole–nanocellulose electrodes. *Journal of Materials Chemistry A*, *2*(21), 7711.

Yuan, L., Yao, B., Hu, B., Huo, K., Chen, W., & Zhou, J. (2013). Polypyrrole-coated paper for flexible solid-state energy storage. *Energy & Environmental Science*, *6*(2), 470 – 476.

Zhang, D., Zhang, Q., Gao, X., & Piao, G. (2013). A Nanocellulose Polypyrrole Composite Based on Tunicate Cellulose. *International Journal of Polymer Science*, *2013*, 6 pages.

Zhang, Y., Nypelö, T., Salas, C., Arboleda, J., Hoeger, I. C., & Rojas, O. J. (2013). Cellulose Nanofibrils: From Strong Materials to Bioactive Surfaces. *Journal of Renewable Materials*, *1*(3), 195–211.

Zheng, G., Cui, Y., Karabulut, E., Wågberg, L., Zhu, H., & Hu, L. (2013). Nanostructured paper for flexible energy and electronic devices. *MRS Bulletin*, *38*(04), 320–325.